RSC Advances

PAPER

View Article Online
View Journal | View Issue

Cite this: *RSC Adv.*, 2024, **14**, 14114

Characteristics of nonconventional hydrogen bonds and stability of dimers of chalcogenoaldehyde derivatives: a noticeable role of oxygen compared to other chalcogens†

Le Thi Tu Quyen,[a] Bui Nhat Tung,[a] Pham Ngoc Thach,[ab] Nguyen Ngoc Tri [ab] and Nguyen Tien Trung *[ab]

In this work, twenty-four stable dimers of RCHZ with R = H, F, Cl, Br, CH_3 or NH_2 and Z = O, S, Se or Te were determined. It was found that the stability of most dimers is primarily contributed by the electrostatic force, except for the dominant role of the induction term in those involving a Te atom, which has been rarely observed. Both electron-donating and -withdrawing groups in substituted formaldehyde cause an increase in the strength of nonconventional C_{sp^2}–H···Z hydrogen bonds, as well as the dimers, in which the electron donating effect plays a more crucial role. The strength of nonconventional hydrogen bonds decreases in the following order: C_{sp^2}–H···O ≫ C_{sp^2}–H···S > C_{sp^2}–H···Se > C_{sp^2}–H···Te. Remarkably, a highly significant role of the O atom compared to S, Se and Te in increasing the C_{sp^2}–H stretching frequency and strength of the nonconventional hydrogen bonds and dimers is found. A C_{sp^2}–H stretching frequency red-shift is observed in C_{sp^2}–H···S/Se/Te, while a blue-shift is obtained in C_{sp^2}–H···O. When Z changes from O to S to Se and to Te, the C_{sp^2}–H blue-shift tends to decrease and eventually turns to a red-shift, in agreement with the increasing order of the proton affinity at Z in the isolated monomer. The magnitude of the C_{sp^2}–H stretching frequency red-shift is larger for C_{sp^2}–H···Te than C_{sp^2}–H···S/Se, consistent with the rising trend of proton affinity at the Z site and the polarity of the C_{sp^2}–H bond in the substituted chalcogenoaldehydes. The C_{sp^2}–H blue-shifting of the C_{sp^2}–H···O hydrogen bonds is observed in all dimers regardless of the electron effect of the substituents. Following complexation, the electron-donating derivatives exhibit a stronger C_{sp^2}–H blue-shift compared to the electron-withdrawing ones. Notably, the stronger C_{sp^2}–H blue-shift turns out to involve a less polarized C_{sp^2}–H bond and a decrease in the occupation at the σ*(C_{sp^2}–H) antibonding orbital in the isolated monomer.

Received 10th March 2024
Accepted 17th April 2024

DOI: 10.1039/d4ra01837k

rsc.li/rsc-advances

1. Introduction

The hydrogen bond is one of the most important weak interactions because of its undeniable role in various fields. The effect of hydrogen bonds is presented in stabilizing chemical structures or the crystal skeleton and participating in biochemical processes.[1–4] Hydrogen bonds are intimately involved in large molecules, such as proteins and nucleic acids, as well as in solvation processes and the function of enzymes.[5,6] The C–H···O/N, C–H···π, and C–H···Y (Y = F, Cl, Br) hydrogen bonds are detected in many clusters, enzyme mechanisms, proteins, DNA, RNA, catalytic reactions, and material structures.[7–12] This indicates the essential role of hydrogen bonds in developing new drugs that serve human health. In addition, organic synthesis methods based on the activation of C–H bonds in intermediate complexes are an attractive topic today because of their importance in controlling the formation of the desired products.[13,14] Notably, the dominant role of hydrogen bonds in the internal cohesion of cellulose microfibrils has also been shown in recent years.[15] In short, the hydrogen bond plays a crucial role in our lives, and understanding the characteristics of hydrogen bonds could help scientists devise a theoretical approach to exploit the application of this weak interaction.

Up to now, hydrogen bonds in the form of X–H···Y have been classified into two types, including conventional and nonconventional hydrogen bonds.[16] The difference between these two types is the electronegativity of the X and Y atoms. X and Y are indeed normally large electronegative atoms, or Y can be a rich

[a]*Laboratory of Computational Chemistry and Modelling (LCCM), Quy Nhon University, 170 An Duong Vuong Street, Quy Nhon City 590000, Vietnam. E-mail: nguyentientrung@qnu.edu.vn*

[b]*Faculty of Natural Sciences, Quy Nhon University, 170 An Duong Vuong Street, Quy Nhon City 590000, Vietnam*

† Electronic supplementary information (ESI) available. See DOI: https://doi.org/10.1039/d4ra01837k

electron density region for conventional hydrogen bonds. Meanwhile, the X and Y atoms in nonconventional hydrogen bonds have much smaller electronegativity. Following complexation, the formation of conventional hydrogen bonds causes an elongation of the X–H bond length and a decrease in its stretching frequency to the red wavelength region, which is called a red-shifting hydrogen bond.[2,17–19] The red shift of the X–H stretching frequency in conventional hydrogen bonds is suggested to be due to a strong electrostatic attraction between H and Y. Remarkably, scientists have found that the stretching frequency of X–H bonds acting as a proton donor in nonconventional hydrogen bonds could shift to red or blue wavelengths upon complexation. This leads to two different properties of nonconventional hydrogen bonds, so-called red-shifting hydrogen bonds and blue-shifting hydrogen bonds. While the former is characterized by the elongation of the X–H bond and the decrease of its stretching frequency,[20] the latter exhibits a bond length contraction and an increase in the stretching frequency of the X–H bond.[21] The red-shift of nonconventional hydrogen bonds is suggested to be due to the intermolecular hyperconjugation effect from n(Y) to the σ*(X–H) orbital overcoming the increase in both *s* character and X–H polarity.[22] The characteristics of the blue-shift, however, have not yet been identified. Several scientists have endeavored to further understand this novel type of hydrogen bond,[23–26] but some controversies regarding the origin of blue-shifting hydrogen bonds have persisted until now. Over the years, various theories and models have been proposed to explain the essence of blue-shifting hydrogen bonds.[27–30] Xin Chang *et al.* suggested that the blue-shift or red-shift relies on the characteristics of the X–H bond, in which the blue-shift is associated with a covalent nature of the X–H bond, while an ionic state of the X–H bond induces a red-shift.[25] Mao and co-workers showed that Pauli repulsion enhances the blue-shift, whereas the merging of electrostatic and dispersion effects causes the red-shift.[31] Another study by Mo suggested that the X–H bond contraction and its blue-shift in the stretching frequency are due to the predominance of long-range electrostatic and Pauli interactions, overcoming the electron density transfer and polarity.[32] In addition, Shaik *et al.* recently reported that valence bond theory could be used to give a generalized description of a hydrogen bond, including the nonconventional C–H···Y hydrogen bonds. Shaik pointed out that the two major interactions that makeup hydrogen bonds are polarization and charge transfer, which are significantly involved in the ionic-valence bond property.[33] In general, these rationalizations have both advantages and disadvantages. However, they explained the origin of nonconventional hydrogen bonds as well as their blue-shift based on complexation without considering the characteristics of the initial proton donors or acceptors and their property relationship. Therefore, studies explaining the characteristics of blue-shifting hydrogen bonds based on the intrinsic properties of the proton donors and acceptors represent potential approaches for understanding nonconventional hydrogen bonds.[34–39] Indeed, Alkorta *et al.*, in their latest report, evaluated the hydrogen bond dissociation energies from the properties of isolated monomers. They suggested that the more negative minimum electrostatic region in a Lewis base (proton acceptor) and the more positive maximum electrostatic one in a Lewis acid (proton donor) cause a stronger hydrogen bond. The increase in the values of the reduced nucleophilicity of the proton acceptor and the reduced electrophilicity of the proton donor also enhance the strength of the hydrogen bond.[40]

Most of the research on blue-shifting hydrogen bonds has investigated the C_{sp^3}–H blue-shift, with the C_{sp^3} atom referring to the tetrahedral hybridized state. For instance, the C–H···Y blue-shifting hydrogen bond was found for the first time in systems between $-CHF_2$ and some proton acceptors in 1980.[21] In 2001, the research group of Reimann reported the C_{sp^3}–H···π hydrogen bond in complexes containing haloforms with benzene derivatives.[41,42] The blue-shifting hydrogen bonds involved in π as a proton donor were also proposed by Oliveira *et al.* in 2009.[43] Besides, the C–H bond contraction during the complexation between a haloform, methane, water, and acetylene was also observed.[44,45] It is noteworthy that the blue-shift of large-polarized C_{sp^2}–H (C_{sp^2} stands for a triangular hybridized carbon atom) created much potential for expanding the research on C_{sp^2}–H···Y hydrogen bonds. The stretching frequency of the C_{sp^2}–H bond can reach 90 cm^{-1} in complexes of formaldehyde and thioformaldehyde with formic acid,[46] which is rarely observed in previous reports. A C_{sp^2}–H blue-shift often appears in the systems of carbonyl compounds, which play an important role in organic reactions and biochemical processes thanks to hydrogen bond formation and proton transfer. Some reports have revealed individual cases of C_{sp^2}–H···O hydrogen bonds between carbonyl derivatives and water.[47–50] Chandra *et al.* explored a large blue-shift of the C_{sp^2}–H···O hydrogen bond with the stretching frequency values changing between 11 and 53 cm^{-1} when investigating the interaction in systems of substituted formaldehyde with some H_2O molecules.[47] Interestingly, the complexation between RCHO and nH_2O/HF (R = H, F, Cl and Li; n = 1–4) in the study by Karpfen demonstrated that the C_{sp^2}–H stretching frequency could be considered for both blue-shift and red-shift.[51] When investigating the interactions in the RCHO dimers with R = H or CH_3 at M062X/6-311++G(3df,3dp), Thakur reported complex stability and the C_{sp^2}–H blue-shift magnitude in the C_{sp^2}–H···O hydrogen bonded interaction is stronger for the CH_3CHO dimer than for the HCHO dimer.[26] This implied the important role of electron-donating substituents in complex stabilization and the C_{sp^2}–H blue-shift. A larger C_{sp^2}–H blue-shift was reported in the complex of HCHO···HCHO compared to HCHO···HCHS and HCHS···HCHS.[49] This shows that the magnitude of C_{sp^2}–H blue-shift in hydrogen bonds depends strongly on the C_{sp^2}–H polarity and the gas-phase basicity of the proton acceptor.

In recent years, proton acceptors containing oxygen and sulfur have been concentrated on for a clearer understanding of the characteristics and nature of nonconventional hydrogen bonds; however, other atoms in the chalcogen series with lower electronegativity are less studied.[52–54] Very recently, the existence of C_{sp}–H and C_{sp^3}–H stretching frequency red-shifts of nonconventional C_{sp}–H···Se and C_{sp^3}–H···Se hydrogen bonds has been theoretically and experimentally discovered in complexes of C_8H_6 and $Se(CH_3)_2$,[55] Q_3CH and SeH_2 (Q = Cl, H,

and F),[56] and $CHCl_3$ and $Se(CH_3)_2$.[57] It is noteworthy that a very large C_{sp^2}–H blue-shift of 104.5 cm^{-1} was reached in the complexes between CH_3CHZ and RCZOH (R = H, CH_3, F; Z = O, S).[54] The nonconventional C_{sp^2}–H···Se/Te and Z–H···Se/Te hydrogen bonds have recently been found in some systems. Indeed, O/N–H···Se/Te hydrogen bonds have been detected through experiments.[58–60] Cuc *et al.* also reported the existence of C_{sp^2}–H···Se/Te hydrogen bonds in the complexes of chalcogenoaldehydes with water or aldehydes with hydrogen chalcogenides.[61,62] It is remarkable that these new hydrogen bonds can belong to either blue- or red-shifting hydrogen bonds. Therefore, the study of C_{sp^2}–H···Se/Te hydrogen bonds is essential to rationalize the origin of blue-shifting hydrogen bonds. Extending the hydrogen bond study to the chalcogen-containing compounds is very consequential for clarifying the nature of hydrogen bonds and their classification.

In the present work, we investigate the interactions in dimers of RCHZ, with R = H, F, Cl, Br, CH_3 or NH_2 and Z = O, S, Se or Te, to shed light on the influence of electron-donating and electron-withdrawing substituents on the stability and characteristics of nonconventional C_{sp^2}–H···Z hydrogen bonds and dimers. A notable role of O compared to other chalcogens in chalcogenoaldehydes in affecting the characteristics and strength of nonconventional hydrogen bonds is also evaluated thoroughly. Furthermore, state-of-the-art chemical quantum approaches are carried out to clarify the existence and strength of hydrogen bonds and dimers, as well as the role of various energetic components in complex stabilization.

2. Computational methods

The second-order perturbation theoretical method (MP2) with the aug-cc-pVTZ-PP basis set for the Te atom and 6-311++G(3df,2pd) for the remaining ones was used for geometry optimizations and harmonic vibrational frequency calculations for isolated monomers and dimers. In order to avoid vibrational coupling between the CH_2 stretching modes in HCHZ (Z = O, S, Se or Te), harmonic frequencies are calculated for the DCHZ isotopomers for both the monomers and complexes. All quantum chemical calculations were performed with the Gaussian 16 suite.[63] The interaction energy of the dimers includes the single-point energy (E), basis set superposition error (BSSE) correction computed at the CCSD(T) level and zero-point energy (ZPE) performed by the MP2 method in combination with the aug-cc-pVTZ-PP basis set for Te and the 6-311++G(3df,2pd) basis set for the remaining atoms. The interaction energies of the dimers (ΔE^*) were calculated as follows:

$$\Delta E^* = (E + \mathrm{ZPE})_{\mathrm{dimer}} - \sum(E + \mathrm{ZPE})_{\mathrm{monomer}} + \mathrm{BSSE}$$

Besides, the deprotonation enthalpy (DPE) of the C_{sp^2}–H bond and the proton affinity (PA) at the Z atom of the isolated monomers were also evaluated using the same level of theory.

The Quantum Theory of Atoms in Molecules (QTAIM)[64,65] was analysed by the AIMall program[66] using the wavefunctions obtained at the MP2/6-311++G(3df,2pd) level, except for the Te atom for which the aug-cc-pVTZ-PP basis set was used, to examine the existence of bond critical points (BCPs), which indicate the presence of hydrogen bonds. Furthermore, the electron density [$\rho(r)$], Laplacian electron density [$\nabla^2(\rho)$], and potential energy density [$V(r)$] at the BCPs were also computed. The individual hydrogen bond energy (E_{HB}) was determined according to the formula of Espinosa–Molins–Lecomte: $E_{HB} = 0.5V(r)$.[67] In addition, Natural Bond Orbital (NBO) analysis was implemented by the NBO 7.0 program at the same level of theory used for AIM analysis to consider the electron transfer and the characteristics of nonconventional hydrogen bonds.[68] The ratio between the H···Z intermolecular distances and their total van der Waals radii ($r_{H\cdots Z}/\sum r_{vdW}$) was additionally calculated to clarify the relationship between intermolecular distance and the strength of nonconventional hydrogen bonds.[69]

Non-Covalent Interaction (NCI) plotting[70] and Molecular Electrostatic Potential (MEP)[71] analysis were also used to determine the properties of the weak interactions in the dimers. The NCI results provide a more intuitive comparison of the non-covalent properties of hydrogen bonds and their stability. MEP analysis is an appropriate approach for understanding molecular reactivity and intermolecular interactions, and recognising the active sites of the monomers. Therefore, in order to visualize the distribution of electron density on the surface of the monomers and determine the electron-rich center on them, we carried out MEP calculations at the MP2/aug-cc-pVTZ-PP level for the Te atom and MP2/6-311++G(3df,2pd) level for the remaining ones. In addition, Symmetry-Adapted Perturbation Theory (SAPT)[72] analysis was performed through the Psi4 program[73] to evaluate the contribution of energy components to the stability of the investigated dimers.

3. Results and discussion

3.1. Geometrical structure and AIM analysis

In order to evaluate the effect of different R and Z substituents on the characteristics and strength of the nonconventional C_{sp^2}–H···Z hydrogen bonds and dimers formed, we first performed geometrical optimization of the HCHZ dimers with Z = O, S, Se or Te, and two stable structures were identified, including the hexagonal (I) and perpendicular (II) forms as shown in Fig. S1 of the ESI.† It is found that structures I with interaction energies in the range of −10.3 to −6.2 kJ mol^{-1} are more stable than structures II (from −9.5 to 2.5 kJ mol^{-1}) (*cf.* Table S1†). Notably, the perpendicular structure of the 2HCHTe dimer exhibits a positive value of the interaction energy. Consequently, only the hexagonal geometry was considered in the dimers of RCHZ, with R = H, F, Cl, Br, CH_3 or NH_2, and Z = O, S, Se or Te. The 24 stable structures of the RCHZ dimers on the potential energy surfaces are displayed in Fig. 1. The dimers are labeled with the name in bold **2R-Z**. In general, these hexagonal ring structures are formed by two C_{sp^2}–H···Z interactions, as confirmed by the ring critical points (RCPs) in the middle of the ring surface (*cf.* Fig. 2). It is noteworthy that the AIM analysis pointed out the presence of bond critical points (BCPs) between two H atoms in the interaction C_{sp^2}–H···H–C_{sp^2} in the **2CH_3/NH_2-Se/Te** dimers (*cf.* Fig. 2). Indeed, the very small electron density [$\rho(r)$] values

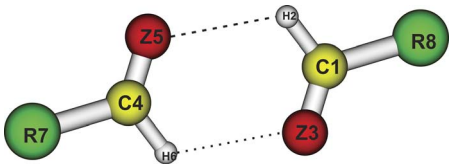

Fig. 1 Stable structures of the dimers between two RCHZ molecules, with R = H, F, Cl, Br or CH_3, and Z = O, S, Se or Te.

ranging from 0.006 au to 0.009 au, along with the positive values of the Laplacian electron density [$\nabla^2(\rho)$] ($\nabla^2(\rho)$ = 0.02–0.04 au) (*cf.* Table S2†) at these BCPs, indicate the existence of very weak C_{sp^2}–H···H–C_{sp^2} dihydrogen bonds in these dimers. This observation is also the reason for the appearance of two RCPs in the **2CH$_3$-Se**, **2CH$_3$-Te**, **2NH$_2$-Se** and **2NH$_2$-Te** dimers.

The ratio between intermolecular distance and the sum of the van der Waals radii of the two interacting atoms ($r_{H\cdots Z}/\sum r_{vdW}$) was calculated and gathered in Table S3.† This parameter is one of the factors that predicts the formation of hydrogen

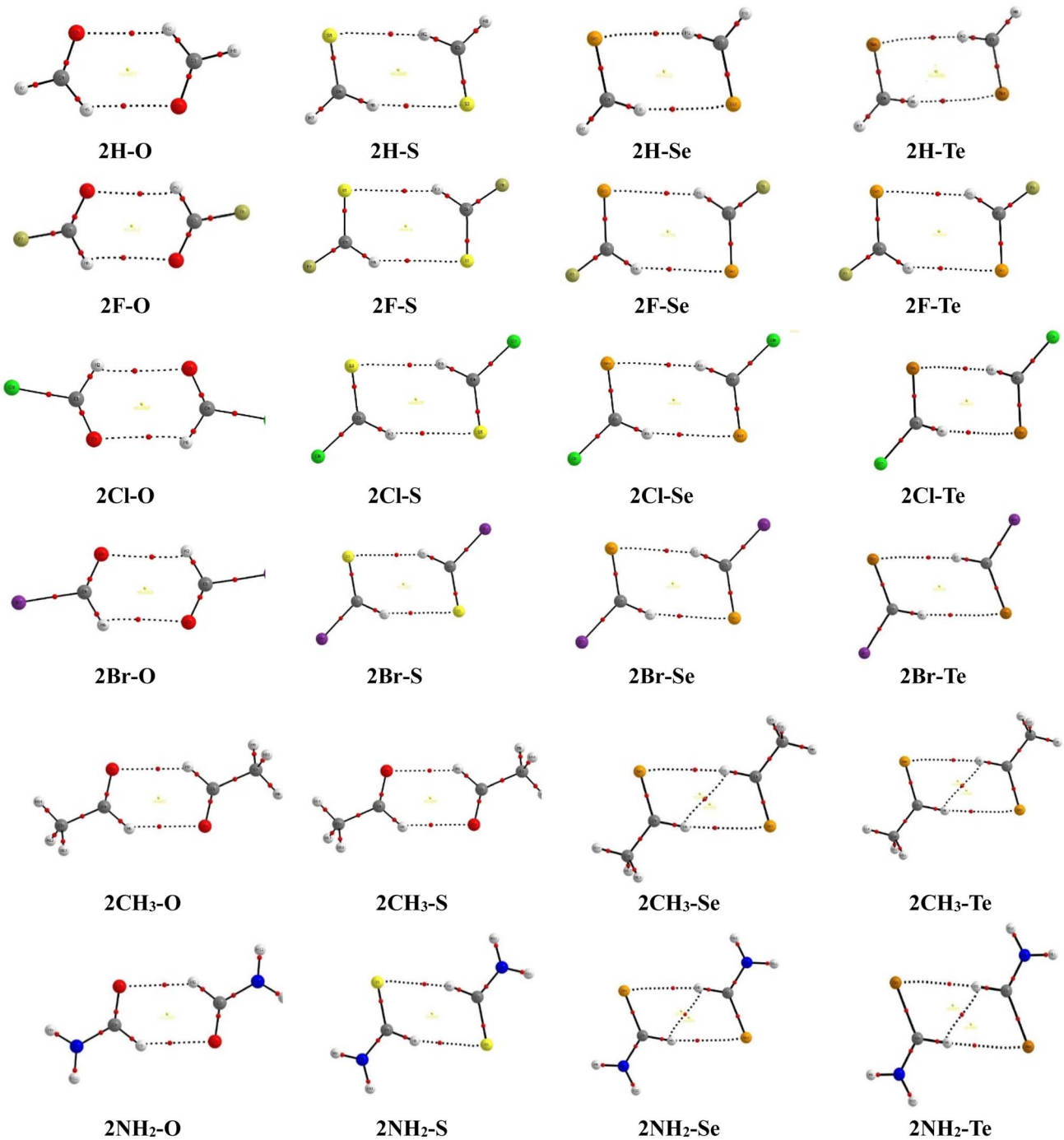

Fig. 2 The topological images of the **2R-Z** dimers with R = H, F, Cl, Br, CH_3 or NH_2 and Z = O, S, Se or Te.

bonds. Thus, the smaller $r_{H\cdots Z}/\sum r_{vdW}$ ratio indicates the stronger H⋯Z interaction, and *vice versa*. Table S3† shows that the $r_{H\cdots Z}/\sum r_{vdW}$ ratios for all intermolecular interactions range from 0.87 to 0.97, indicating the smaller value of H⋯Z distance compared to the sum of the van der Waals radii. These ratios imply the existence of C_{sp^2}–H⋯O/S/Se/Te nonconventional hydrogen bonds in the dimers, which is evidenced by the presence of BCPs between the interacting atoms given in Fig. 2. The $\rho(r)$ and $\nabla^2(\rho)$ values at the BCPs are in the ranges of 0.008–0.012 au and 0.02–0.04 au, respectively (*cf.* Table S3†). These values belong to the regions of weak non-covalent interactions.[74] Besides, the individual hydrogen bond energies (E_{HB}) in the dimers have negative values, indicating the stability of all of the formed nonconventional hydrogen bonds, including C_{sp^2}–H⋯O, C_{sp^2}–H⋯S, C_{sp^2}–H⋯Se, and C_{sp^2}–H⋯Te.

There is a good agreement between the $r_{H\cdots Z}/\sum r_{vdW}$ ratios and the strength of the hydrogen bonds, which is presented by the relationship between the $r_{H\cdots Z}/\sum r_{vdW}$ ratios and E_{HB} values in Fig. 3. For the same R, the $r_{H\cdots Z}/\sum r_{vdW}$ ratio increases in the order of substituents O < S < Se < Te, indicating that the C_{sp^2}–H⋯O hydrogen bonds are more stable than the C_{sp^2}–H⋯S/Se/Te ones. The E_{HB} values of the C_{sp^2}–H⋯O hydrogen bonds (from −8.1 kJ mol^{-1} to −11.0 kJ mol^{-1}) are indeed more negative than those of C_{sp^2}–H⋯S/Se/Te (from −4.7 kJ mol^{-1} to −9.3 kJ mol^{-1}). This tendency was also observed in complexes of XCHO and H_2Y with X = H, F, Cl, Br or CH_3 and Y = O, S, Se or Te, in which the E_{HB} values of the C_{sp^2}–H⋯O and C_{sp^2}–H⋯S/Se/Te hydrogen bonds at the MP2/aug-cc-pVDZ level are in the ranges from −10.2 to −11.2 kJ mol^{-1} and from −3.7 to −5.5 kJ mol^{-1}, respectively.[62] This is due to the larger negative value of $V_{S,min}$ at the O atom in XCHO (−108.3 to −193.1 kJ mol^{-1}) compared to the S, Se and Te atoms in other monomers (−70.9 to −131.0 kJ mol^{-1}) (*cf.* Table S4, Fig. S2†), which is in line with a decrease of notable electronegativity from O (3.44) to S (2.58) *via* Se (2.55) and then to Te (2.10). Consequently, the electronegativity of chalcogen Z atoms in the monomers acts as an important factor in the stability of nonconventional C_{sp^2}–H⋯Z hydrogen bonds, especially a crucial role of the O atom relative to the S, Se and Te ones. The effect of electronegativity on the strength of the hydrogen bonds was also suggested by Liu *et al.* when investigating the dimers between H_2Y and HX (X= F, Cl, Br; Y = O, S, Se) at the MP2/aug-cc-pVTZ level.[39]

When keeping Z and changing the R substituents, the change in the strength of the nonconventional C_{sp^2}–H⋯Z hydrogen bonds in the **2R-O** dimers has a very distinct tendency as compared to those in the **2R-S/Se/Te** ones (*cf.* Fig. 3). For Z = O, the $r_{H\cdots Z}/\sum r_{vdW}$ values in the dimers containing electron-donating and -withdrawing groups are smaller than those in the dimer of formaldehyde. The strength of the nonconventional C_{sp^2}–H⋯O hydrogen bonds decreases in the sequence of substituents NH_2 > CH_3 > F/Cl/Br > H, in accordance with a decrease in the PA values at the O sites in the isolated monomers (*cf.* Table 1). For Z = S, Se and Te, the more stable hydrogen bonds in **2NH$_2$/CH$_3$-S/Se/Te** and **2Cl/Br-S/Se/Te** compared to **2H-S/Se/Te** exhibit a smaller $r_{H\cdots Z}/\sum r_{vdW}$ ratio, except for **2F-S/Se/Te**. Besides, larger $r_{H\cdots Z}/\sum r_{vdW}$ values are found for **2CH$_3$-S/Se/Te** than for the **2Cl/Br-S/Se/Te** ones. This observation shows a decrease in the strength of nonconventional C_{sp^2}–H⋯S/Se/Te hydrogen bonds in the order of **2NH$_2$-Z** > **2Br-Z** ∼ **2Cl-Z** > **2CH$_3$-Z** > **2H-Z** > **2F-Z**, with Z = S, Se and Te.

3.2. Interaction energy and SAPT2+ analysis

To investigate the stability of the dimers and the factors impacting their strength, the interaction energies with both ZBE and BSSE corrections of 24 dimers are calculated and given in Table 2. The data show that the interaction energies of all dimers have negative values from −6.2 to −21.2 kJ mol^{-1}, implying their strength on the potential energy surface. Among them, the most negative values belong to **2NH$_2$-Z**, 2–3 times as negative as those of **2H-Z**. The considerable strength of complexes containing the NH_2 group was also obtained in the interactions of XCHY with HCOOH (X = H, F, Cl, Br, CH_3, NH_2 and Y=O, S), with the interaction energies from −15.3 kJ mol^{-1} to −42.2 kJ mol^{-1} at the CCSD(T)/aug-cc-pVDZ//MP2/aug-cc-pVDZ level.[46]

As seen in Table 2, for the same R = H, F, Cl, Br and CH_3, the stability of the **2R-O** dimers is larger than that of the **2R-S/Se/Te** ones, which is due to the ΔE^* values being from −10.3 to −13.6 kJ mol^{-1} for **2R-O** and from −6.2 to −11.5 kJ mol^{-1} for **2R-S/Se/Te**, consistent with the more negative charges at O compared to S, Se and Te (*cf.* Table S5†), affirming the greater importance of the O than S, Se and Te ones for the stabilization of the dimers. Van Dornshuld also highlighted the greater strength of $(CH_2O)_2$ in comparison with $(CH_2S)_2$.[49] Regarding the **2NH$_2$-Z** dimers, it is noted that the interaction energies of **2NH$_2$S/Se/Te** are more negative than those of **2NH$_2$-O**. In comparison with **2R-Z** (R = H, F, Cl, Br or CH_3 and Z = O, S, Se or Te), the difference in negative charges at the O, S, Se and Te atoms in **2NH$_2$-Z** is negligible (*cf.* Table S5†). However, the intermolecular electron density transfer from the n(Z) to σ*(C1–H2) orbital in **2NH$_2$-S/Se/Te** (12.5–15.7 kJ mol^{-1}) is much larger than that in **2NH$_2$-O** (9.6 kJ mol^{-1}) (*cf.* Table 3). This leads to a larger strength of **2NH$_2$-S/Se/Te** compared to **2NH$_2$-O**.

For Z = O, the descending interaction energy values display an increase in the dimer stability in the order of **2H-O** < **2CH$_3$-O** < **2F-O** ∼ **2Cl-O** ∼ **2Br-O** < **2NH$_2$-O**. It is notable that the **2F/Cl/Br-O** dimers (ΔE^* being from −13.2 to −13.6 kJ mol^{-1}) are more stable than **2CH$_3$-O** (ΔE^* being −12.0 kJ mol^{-1}), while they are less stable than **2NH$_2$-O**. The larger positive resonance effect of NH_2 compared to the hyperconjugation effect of CH_3 leads to stronger electron-donating ability of NH_2 relative to the CH_3 group. In addition, the larger proton affinity at O in NH_2CHO compared to the remaining monomers (*cf.* Table 1) also contributes to the strongest stability of the **2NH$_2$-O** dimer. On the other hand, the strength tendency of the **2R-O** dimers implies a large role of C_{sp^2}–H polarity relative to proton affinity at the O site in substituted formaldehyde in stabilizing the dimers. The magnitude and changing tendency of PA at the O site and DPE of the C_{sp^2}–H in the isolated monomers are the reason for this strength ordering (*cf.* Table 1). The stronger strength of 2F/Cl/Br–O dimers compared to the $2CH_3$–O one is due to the larger polarity of the C_{sp^2}–H bond in F/Cl/BrCHO relative to CH_3CHO, and even surpasses the proton affinity at

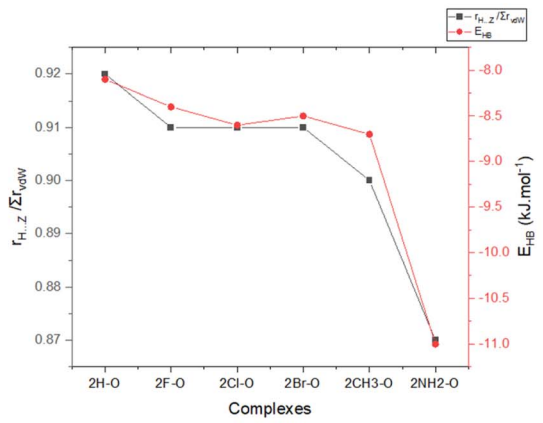

2R-O

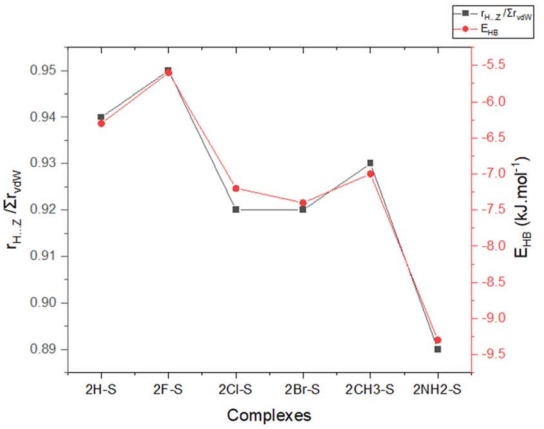

2R-S

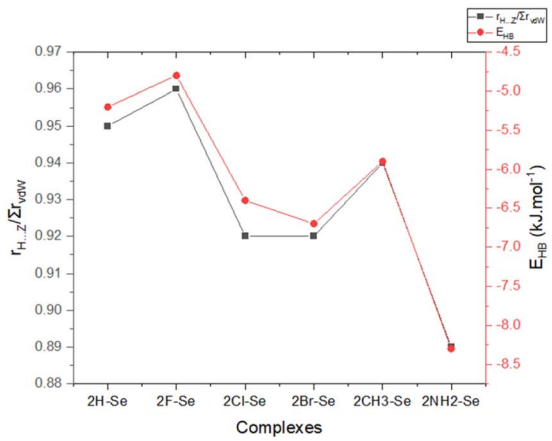

2R-Se

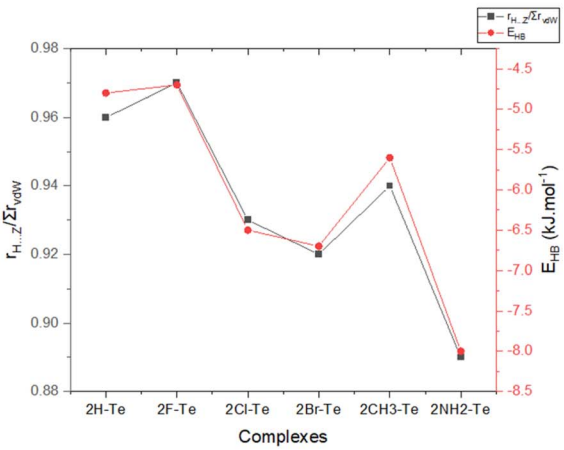

2R-Te

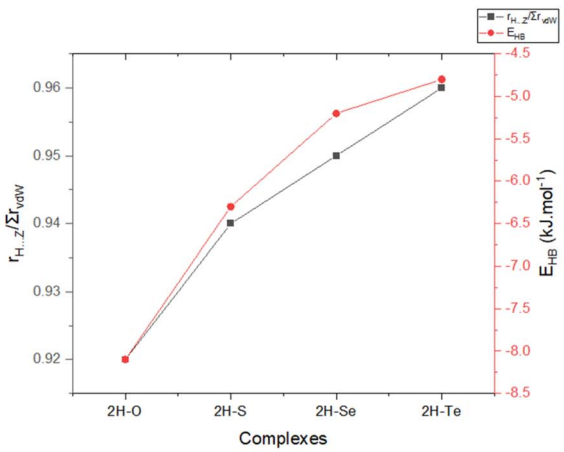

2H-Z

Fig. 3 The relationship between the $r_{H\cdots Z}/\sum r_{vdW}$ ratios and individual hydrogen bond energy (E_{HB}) in the **2R-Z** dimers (R = H, F, Cl, Br or CH_3; Z = O, S, Se or Te).

Table 1 Deprotonation enthalpies (DPEs) of the C_{sp^2}–H bond in the RCHZ monomers and the proton affinities (PA) at the Z site of RCHZ, with R = H, F, Cl, Br, CH_3 or NH_2, and Z= O, S, Se or Te

	HCHO[a]	HCHS	HCHSe	HCHTe
DPE(C_{sp^2}–H) (kJ mol^{-1})	1684.9	1636.5	1625.9	1611.4
PA(Z) (kJ mol^{-1})	696.6	753.1	754.2	770.2
	FCHO	FCHS	FCHSe	FCHTe
DPE(C_{sp^2}–H) (kJ mol^{-1})	1583.8	1581.3	1571.2	1560.1
PA(Z) (kJ mol^{-1})	642.2	706.8	716.9	740.0
	ClCHO	ClCHS	ClCHSe	ClCHTe
DPE(C_{sp^2}–H) (kJ mol^{-1})	1540.9	1557.7	1554.6	1549.7
PA(Z) (kJ mol^{-1})	678.2	739.3	744.8	761.7
	BrCHO	BrCHS	BrCHSe	BrCHTe
DPE(C_{sp^2}–H) (kJ mol^{-1})	1505.0	1542.0	1542.2	1540.8
PA(Z) (kJ mol^{-1})	682.5	746.1	751.3	766.9
	CH_3CHO[b]	CH_3CHS	CH_3CHSe	CH_3CHTe
DPE(C_{sp^2}–H) (kJ mol^{-1})	1659.9	1629.1	1623.5	1614.4
PA(Z) (kJ mol^{-1})	755.6	793.4	791.4	801.2
	NH_2CHO	NH_2CHS	NH_2CHSe	NH_2CHTe
DPE(C_{sp^2}–H) (kJ mol^{-1})	1632.8	1592.6	1575.4	1557.2
PA(Z) (kJ mol^{-1})	873.1	888.2	882.7	909.5

[a] $DPE_{experiment}(C_{sp^2}–H) = 1650.7$ (kJ mol^{-1})[75] and $PA_{experiment}$ (O) = 712.9 (kJ mol^{-1})[76] in HCHO molecule. [b] $DPE_{experiment}(C_{sp^2}–H) = 1645.1$ (kJ mol^{-1})[77] and $PA_{experiment}$ (O) = 768.5 (kJ mol^{-1})[78] in CH_3CHO molecule.

Table 2 Interaction energies corrected by ZPE and BSSE (ΔE^*, kJ mol^{-1}) of the **2R-Z** dimers (R = H, F, Cl or CH_3; Z = O, S, Se or Te)

Complex	ΔE^*	Complex	ΔE^*	Complex	ΔE^*	Complex	ΔE^*
2H-O	−10.3	**2H-S**	−7.3	**2H-Se**	−7.9	**2H-Te**	−6.2
2F-O	−13.6	**2F-S**	−8.6	**2F-Se**	−9.7	**2F-Te**	−9.0
2Cl-O	−13.5	**2Cl-S**	−9.3	**2Cl-Se**	−10.6	**2Cl-Te**	−9.4
2Br-O	−13.2	**2Br-S**	−9.9	**2Br-Se**	−10.9	**2Br-Te**	−9.1
2CH_3-O	−12.0	**2CH_3-S**	−10.8	**2CH_3-Se**	−11.5	**2CH_3-Te**	−9.7
2NH_2-O	−17.7	**2NH_2-S**	−19.1	**2NH_2-Se**	−21.2	**2NH_2-Te**	−21.0

O in CH_3CHO. The notable importance of C_{sp^2}–H polarity in stabilizing the **2R-Z** dimer is different from the dominant role of O–H polarity in both HCOOH and H_2O,[46,61] overcoming the proton affinity of O in CH_3CHO and F/Cl/BrCHO in determining the strength of the complexes.

For Z = S, Se and Te, the strength of the dimers increases in the sequence of **2H-Z** < **2F-Z** < **2Cl-Z** ∼ **2Br-Z** < **2CH_3-Z** < **2NH_2-Z,** in which a considerable stability of the dimer is found as Z = NH_2 compared to the remaining substituents (*cf.* Table 2). This indicates that one H in HCHZ substituted by the electron-donating group leads to a larger increase in the strength of the **2R-Z** dimers as compared to that by the electron-

Table 3 The NBO analysis of the **2R-Z** dimers, with R = H, F, Cl, Br, CH_3 or NH_2 and Z = O, S, Se or Te

	2H-O	**2H-S**	**2H-Se**	**2H-Te**
E_{inter}[n(Z5) → σ*(C_{sp^2}–H)][a] (kJ mol^{-1})	4.1	8.6	7.5	5.9
E_{intra}[n(Z3) → σ*(C_{sp^2}–H)][b] (kJ mol^{-1})	102.7	59.1	50.8	39.7
$\sum E_{inter}$[c] (kJ mol^{-1})	4.1	8.6	7.5	6.5
ΔE_{intra}[d] (kJ mol^{-1})	−11.9	−4.7	−2.4	0.7
$\Delta\sigma^*(C_{sp^2}–H)$ (10^{-3} e)	−4.4	0.5	1.3	1.8
Δ%*s*(C)	0.8	0.96	0.86	0.71
	2F-O	**2F-S**	**2F-Se**	**2F-Te**
E_{inter}[n(Z5) → σ*(C_{sp^2}–H)][a] (kJ mol^{-1})	4.4	10.3	9.7	9.0
E_{intra}[n(Z3) → σ*(C_{sp^2}–H)][b] (kJ mol^{-1})	100.9	62.6	48.0	34.9
$\sum E_{inter}$[c] (kJ mol^{-1})	4.4	10.3	9.8	9.9
ΔE_{intra}[d] (kJ mol^{-1})	−9.4	−6.9	−3.4	−4.4
$\Delta\sigma^*(C_{sp^2}–H)$ (10^{-3} e)	−3.0	0.5	1.3	2.0
Δ%*s*(C)	0.5	0.8	0.9	0.9
	2Cl-O	**2Cl-S**	**2Cl-Se**	**2Cl-Te**
E_{inter}[n(Z5) → σ*(C_{sp^2}–H)][a] (kJ mol^{-1})	3.5	12.2	11.9	10.2
E_{intra}[n(Z3) → σ*(C_{sp^2}–H)][b] (kJ mol^{-1})	114.2	70.1	54.3	40.8
$\sum E_{inter}$[c] (kJ mol^{-1})	3.5	12.2	11.9	11.8
ΔE_{intra}[d] (kJ mol^{-1})	−9.8	−7.5	−6.0	−3.9
$\Delta\sigma^*(C_{sp^2}–H)$ (10^{-3} e)	−3.5	0.5	1.6	2.9
Δ%*s*(C)	0.5	1.0	1.1	1.0
	2Br-O	**2Br-S**	**2Br-Se**	**2Br-Te**
E_{inter}[n(Z5) → σ*(C_{sp^2}–H)][a] (kJ mol^{-1})	2.7	11.7	11.3	9.5
E_{intra}[n(Z3) → σ*(C_{sp^2}–H)][b] (kJ mol^{-1})	115.0	71.7	56.3	43.2
$\sum E_{inter}$[c] (kJ mol^{-1})	2.7	11.7	11.3	11.4
ΔE_{intra}[d] (kJ mol^{-1})	−9.8	−7.5	−5.3	−2.8
$\Delta\sigma^*(C_{sp^2}–H)$ (10^{-3} e)	−3.5	0.3	1.5	3.0
Δ%*s*(C)	0.5	1.1	1.2	1.0
	2CH_3-O	**2CH_3-S**	**2CH_3-Se**	**2CH_3-Te**
E_{inter}[n(Z5) → σ*(C_{sp^2}–H)][a] (kJ mol^{-1})	5.8	9.3	7.8	5.9
E_{intra}[n(Z3) → σ*(C_{sp^2}–H)][b] (kJ mol^{-1})	115.6	68.9	54.8	42.7
$\sum E_{inter}$[c] (kJ mol^{-1})	6.1	9.3	8.0	6.8
ΔE_{intra}[d] (kJ mol^{-1})	−15.2	−4.7	−2.2	1.5
$\Delta\sigma^*(C_{sp^2}–H)$ (10^{-3} e)	−5.3	0.4	1.3	2.2
Δ%*s*(C)	0.9	1.0	0.9	0.7
	2NH_2-O	**2NH_2-S**	**2NH_2-Se**	**2NH_2-Te**
E_{inter}[n(Z5) → σ*(C_{sp^2}–H)][a] (kJ mol^{-1})	9.6	15.7	15.0	12.5
E_{intra}[n(Z3) → σ*(C_{sp^2}–H)][b] (kJ mol^{-1})	113.2	66.7	51.3	38.4
$\sum E_{inter}$[c] (kJ mol^{-1})	9.9	15.8	15.5	15.4
ΔE_{intra}[d] (kJ mol^{-1})	−20.0	−7.5	−5.0	−1.9
$\Delta\sigma^*(C_{sp^2}–H)$ (10^{-3} e)	−5.8	1.7	3.4	4.9
Δ%*s*(C)	1.0	1.3	1.2	1.1

[a] The hyperconjugative interaction energy of the intermolecular electron transfer from lone pair n(Z5) to the σ*(C_{sp^2}–H) orbital. [b] The hyperconjugative interaction energy of the intramolecular electron transfer from lone pair n(Z3) to the σ*(C_{sp^2}–H) orbital. [c] The total hyperconjugative interaction energies of the intermolecular electron transfers to the σ*(C_{sp^2}–H) orbital. [d] The change in energy of the intramolecular electron transfers to the σ*(C_{sp^2}–H) orbital.

withdrawing group. Accordingly, for Z = S, Se and Te, the strength of **2R-Z** is contributed by both C_{sp^2}–H polarity and proton affinity at the Z site in the monomers, in which a larger role of the latter relative to the former is proposed.

A SAPT2+ analysis was carried out using the def2-TZVPD basis set to clarify the role of the energetic components in the dimer stabilization. The obtained data are gathered in Table S6† and visualized in Fig. 4. The **2R-O/S/Se** dimers are stabilized by three main components: electrostatic, dispersion and induction terms. The contribution of the electrostatic component is the largest (32.0–54.5%), surpassing the two remaining terms, including the induction (16.3–54.2%) and the dispersion (0.2–32.7%). The percentage of electrostatic terms for **2R-O** is much higher than those for **2R-S/Se/Te**, indicating the significant contribution of the electrostatic component to the stability of **2R-O** compared to **2R-S/Se/Te**. The contributing percentage of the dispersion and induction terms in **2R-Z** is negligibly changed as Z goes from O *via* S to Se, while they shift quickly for **2R-Te**. Remarkably, the induction component is *ca.* 52% and the dispersion decreases suddenly to *ca.* 1.0% in the **2R-Te** dimers (*cf.* Table S6†). Therefore, the strength of **2R-Te** is contributed by both induction and electrostatic terms, in which a larger contribution of the former is observed. This observation is confirmed when the SAPT2+ calculations for **2R-Te** are recalculated using different basis sets, including def2-TZVPPD for all atoms, def2-TZVPPD for the Te atom and aug-cc-pVTZ for the remaining ones, and def2-QZVPPD for all atoms (*cf.* Table S7 and Fig. S3a and b†).

3.3. NBO and NCI analysis

NBO analysis was conducted to gain a clearer view of the intermolecular electron density transfer and electron distribution during the formation of dimers. The selected data are given in Table 3.

As seen in Table 3, for the same R, the intermolecular hyperconjugative interaction energies of n(Z5) → σ*(C_{sp^2}–H) increase considerably when replacing the O in **2R-O** by S, Se, and Te. This result is in line with the smaller value for E_{inter}[n(O) → σ*(C_{sp^2}–H)] than E_{inter}[n(S/Se/Te) → σ*(C_{sp^2}–H)] in the XCHO···nH_2Z complexes with X = H, F, Cl, Br or CH_3, Z = O, S, Se or Te and n = 1–2, calculated at the ωB97X-D/aug-cc-pVDZ level.[62] It is noteworthy that there is a significant decrease in the total intramolecular interaction energies of electron transfers from n(O), π(C=O) and σ(C-R) to the σ*(C_{sp^2}–H) orbital (from −20.0 kJ mol^{-1} to −9.4 kJ mol^{-1}) in the **2R-O** dimers, overcoming their total intermolecular hyperconjugative interaction energies (from 2.7 kJ mol^{-1} to 9.9 kJ mol^{-1}). This implies a significant contribution of intramolecular electron transfer to the rearrangement of the electron density in the RCHO monomers during the complexations, leading to a decrease in occupation at the σ*(C_{sp^2}–H) orbital of **2R-O**. In contrast, positive values of Δσ*(C_{sp^2}–H) are obtained in the dimers of **2R-S/Se/Te** because of the dominance of the hyperconjugative interaction energies over the decrease in intramolecular interaction energy. Indeed, the $\sum E_{inter}$ and ΔE_{intra} values of the electron transfers in **2R-S/Se/Te** are in the ranges from 6.5 to 15.8 kJ mol^{-1} and from −7.5 to 1.5 kJ mol^{-1}, respectively. These data lend support to a prediction that a strong C_{sp^2}–H blue-shift is observed for the C_{sp^2}–H···O, while a C_{sp^2}–H red-shift is found for C_{sp^2}–H···S/Se/Te. Despite the smaller intermolecular electron density transfer from n(O) relative to that from n(S/Se/Te) to the σ*(C_{sp^2}–H) orbital, the C_{sp^2}–H···O is more stable than the C_{sp^2}–H···S/Se/Te due to the highly negative charge density on the O site (*cf.* Table S5†). Therefore, the strength of nonconventional C_{sp^2}–H···Z hydrogen bonds is contributed by both intermolecular electron density transfer and electrostatic attraction, in which a more dominant role of the latter is presented.

For Z = O, the intermolecular electron density transfer from n(O) to the σ*(C_{sp^2}–H) orbital in the dimers containing electron-donating substituents is stronger than in those with electron-withdrawing ones. Furthermore, the Δσ*(C_{sp^2}–H) values become less negative in the order of **2NH$_2$-O** ∼ **2CH$_3$-O** > **2H-O** > **2Cl/Br/F-O**, corresponding to the more significantly negative ΔE_{intra} of the **2NH$_2$/CH$_3$-O** dimers than the **2H-O** and **2Cl/Br/F-O** ones (*cf.* Table 3). This indicates that the greater contribution of electron-donating groups relative to electron-withdrawing ones exhibits an enhancement of the C_{sp^2}–H blue-shift. Regarding Z = S, Se and Te, the E_{inter} values of n(Z5) → σ*(C_{sp^2}–H) descend in the order of the substituents NH_2 > Cl ∼ Br > F > CH_3 > H, implying that the electron density transfer from n(Z5) to the σ*(C_{sp^2}–H) orbital in the **2R-S/Se/Te** dimers lessens along that order.

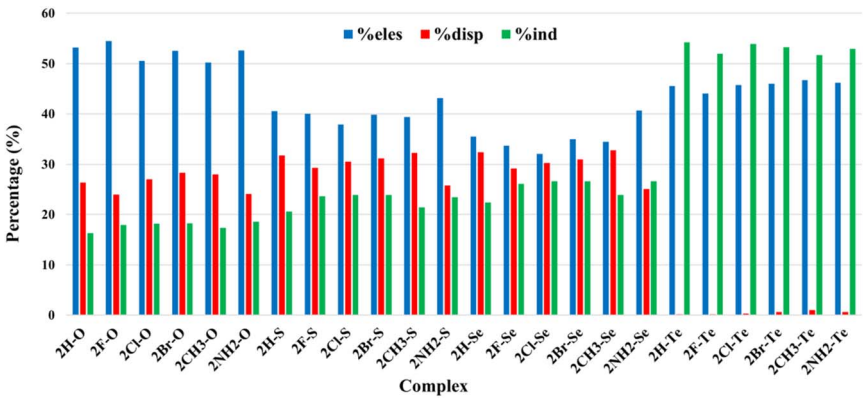

Fig. 4 The percentage contribution (%) of the energy components to the stability of the **2R-Z** dimers at the def2-TZVPD level, with R = H, F, Cl, Br, CH_3 or NH_2 and Z = O, S, Se or Te.

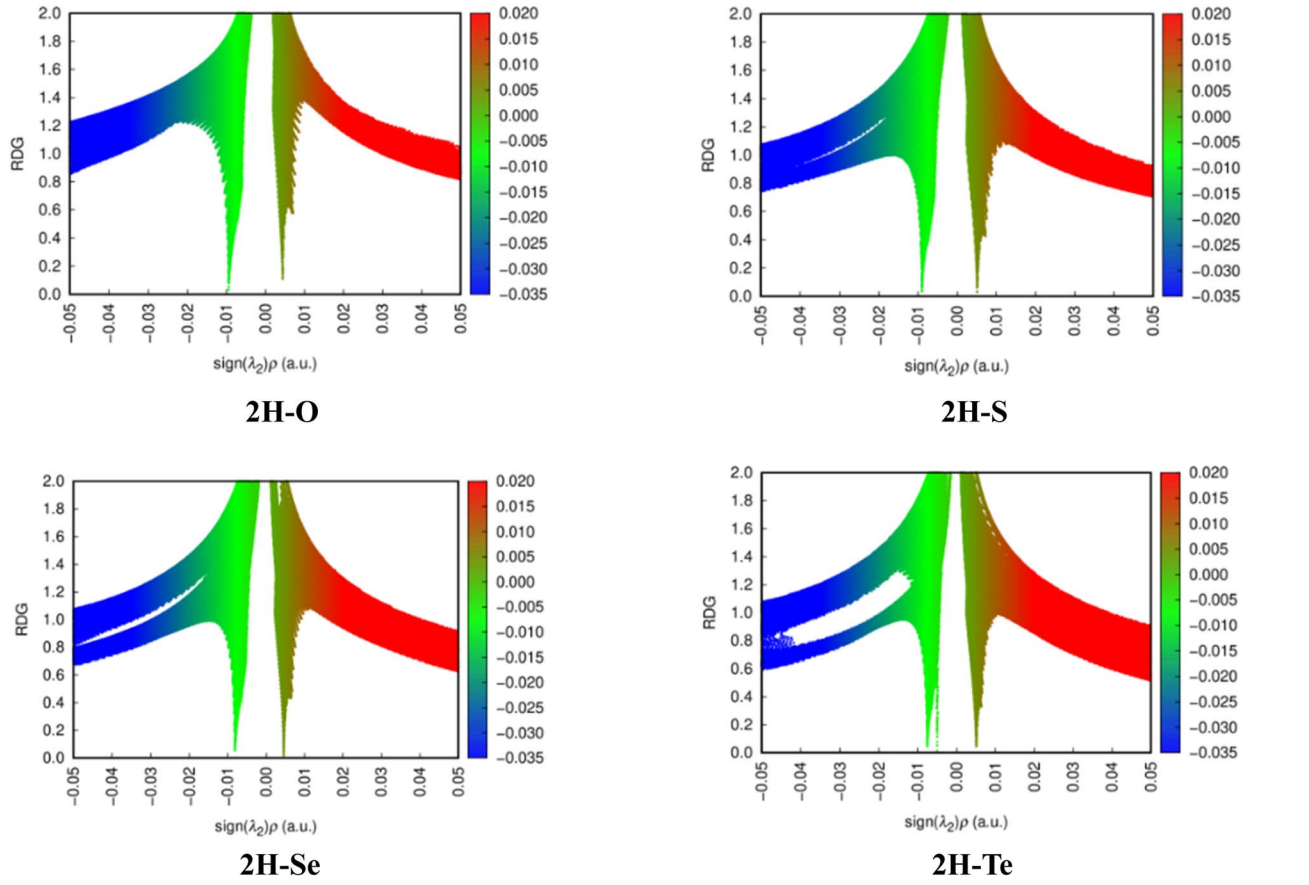

Fig. 5 Plots of the reduced density gradient (*s*, au) *versus* the electron density multiplied by the sign of the second Hessian eigenvalue (sign(λ_2)ρ, au) for the **2H-Z** dimers (Z = O, S, Se or Te).

In addition, the results from the NCI plot (*cf.* Fig. 5 and S4a, b, and Table S8†) show that the reduced density gradient (RDG) of C_{sp^2}–H···Z interaction spikes ranges from 0.086 to 0.179 au (RDG $\approx$ 0), confirming that the nonconventional C_{sp^2}–H···Z hydrogen bonds in the dimers belong to weak non-covalent interactions (*cf.* Table S8†). For the same R, the spikes of the C_{sp^2}–H···O hydrogen bonds are located in a more negative region of sign(λ_2)$\rho(r)$ as compared to those of the C_{sp^2}–H···S/Se/Te ones, validating the more attractive interaction of the C_{sp^2}–H···O hydrogen bonds. For Z= O, the most negative sign(λ_2)$\rho(r)$ regions of C_{sp^2}–H···O are observed for the spikes of **2NH$_2$-O** (sign(λ_2)$\rho(r)$ = −0.0119 au), and the least negative ones belong to the spikes of **2H-O** (sign(λ_2)$\rho(r)$ = −0.0095 au). In the case of Z= S, Se and Te, the spikes of C_{sp^2}–H···S/Se/Te tend to the left as R goes from F/H to CH_3 to Cl/Br and then to NH_2, confirming the increase in the strength of the hydrogen bonds in the order of substituents F ~ H < CH_3 < Cl ~ Br < NH_2, as found from the AIM analysis.

3.4. Changes in the C_{sp^2}–H bond lengths and their stretching frequencies

The changes in the C_{sp^2}–H bond lengths and their stretching frequencies in the **2R-Z** dimers compared to the relevant RCHZ monomers are calculated to evaluate the characteristics of the nonconventional C_{sp^2}–H···Z hydrogen bonds. The obtained results are gathered in Fig. 6 and Table S9.† The results show that the changes in the stretching frequencies of the C_{sp^2}–H bonds are negative with the values from −0.3 to −38.6 cm^{-1}, along with the C_{sp^2}–H elongation of 0.3–2.4 mÅ for the **2R-S**, **2R-Se** and **2R-Te** dimers (*cf.* Table S9†), demonstrating the C_{sp^2}–H stretching frequency red-shift of the nonconventional C_{sp^2}–H···S/Se/Te hydrogen bonds. The C_{sp^2}–H red-shift of the nonconventional

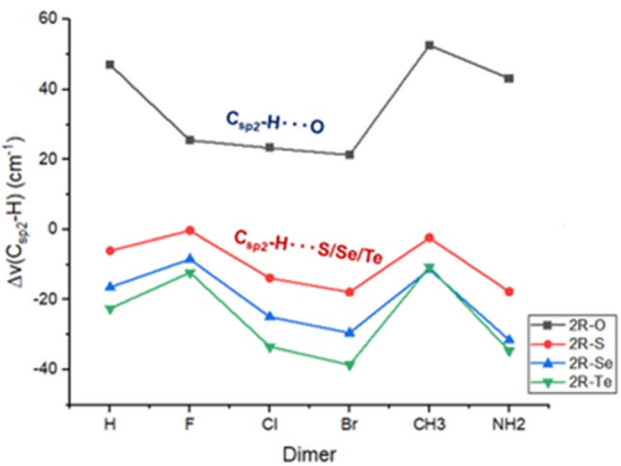

Fig. 6 The tendency of red-shifting and blue-shifting of the nonconventional C_{sp^2}–H···Z hydrogen bonds in the **2R-Z** dimers with R = H, F, Cl, Br, CH_3 or NH_2 and Z = O, S, Se or Te.

C_{sp^2}–H···Se hydrogen bonds in the $[C_8H_8\cdots Se(CH_3)_2]$ complex has been recently determined by the experimental and theoretical results of 101 cm^{-1} and 89 cm^{-1}, respectively.[55] It was reported that the C_{sp^2}–H···S/Se/Te hydrogen bonds were red-shifted up to 36.1 cm^{-1} in the complexes of aldehydes and hydrogen chalcogenides, in which the blue-shift of C_{sp^2}–H···Te is stronger than that of C_{sp^2}–H···S/Se.[62] Conversely, the C_{sp^2}–H blue-shift is observed in the nonconventional C_{sp^2}–H···O hydrogen bonds with the values of $\Delta\nu(C_{sp^2}\text{–H})$ and $\Delta r(C_{sp^2}\text{–H})$ from 21.3 to 52.6 cm^{-1} and from −3.5 to −0.9 mÅ, respectively (*cf.* Table S9†). The difference in the characteristics between C_{sp^2}–H···S/Se/Te and C_{sp^2}–H···O hydrogen bonds results from the greater role of the noticeable intermolecular transfer of electron density from n(S/Se/Te) to the $\sigma^*(C_{sp^2}\text{–H})$ orbital compared to that from n(O) to the $\sigma^*(C_{sp^2}\text{–H})$ one. This highlights a noticeably different role of O compared to S, Se, and Te in changing the C_{sp^2}–H bond length and its stretching frequency upon complexation.

The enhancement of the electron density occupation at the $\sigma^*(C_{sp^2}\text{–H})$ orbital (*cf.* Table 3) leads to an increase in C_{sp^2}–H bond length and a decrease in its stretching frequency in the C_{sp^2}–H···S/Se/Te hydrogen bonds. For the same R, the C_{sp^2}–H red-shift of the stretching frequency decreases in the sequence of C_{sp^2}–H···Te > C_{sp^2}–H···Se > C_{sp^2}–H···S following complexation (*cf.* Fig. 6). The larger $\Delta\sigma^*(C_{sp^2}\text{–H})$ values (*cf.* Table 3) indeed lead to an increase in the $\Delta r(C_{sp^2}\text{–H})$ values as Z changes from S to Te, which is accompanied by the more negative $\Delta\nu(C_{sp^2}\text{–H})$ values in this order. This tendency of C_{sp^2}–H red-shift is in good agreement with the increase in the proton affinity at the S/Se/Te site and the more polarization of the C_{sp^2}–H bonds in the sequence of isolated monomers RCHS < RCHSe < RCHTe. For the same Z being S, Se and Te, the $\Delta\nu(C_{sp^2}\text{–H})$ values of the C_{sp^2}–H bond become more negative in the order of substituents F < CH_3 < H < Cl < Br ∼ NH_2 (*cf.* Fig. 6), indicating the enhancement of the C_{sp^2}–H red-shift in the nonconventional C_{sp^2}–H···S/Se/Te hydrogen bonds according to this trend. Therefore, the rule of the effect of electron-donating and withdrawing groups on the characteristics of C_{sp^2}–H···S/Se/Te should not be presented in the **2R-S/Se/Te** dimers. The reason for its characteristics could be suggested by the rearrangement of the electron density during the formation of the dimers.

For Z = O, the blue-shift of the nonconventional C_{sp^2}–H···O hydrogen bonds is proposed by the considerable decrease in the occupation of the $\sigma^*(C_{sp^2}\text{–H})$ orbital upon complexation, leading to the contraction of the C_{sp^2}–H bond and an increase in its stretching frequencies. Indeed, the stretching frequency blue-shifts of the C_{sp^2}–H bond in the **2R-O** dimers are found to lie between 21 cm^{-1} and 53 cm^{-1} (*cf.* Table S9†). The approximate C_{sp^2}–H blue-shifts of the C_{sp^2}–H···O hydrogen bonds were reported in the YCHO···H_2O complexes (Y = H, F, Cl, Br, or CH_3) with the values of $\Delta\nu(C_{sp^2}\text{–H})$ being 21–52 cm^{-1}.[61] For the complexes of XCHO (X = H, F and Cl) with H_2O, the blue-shifts of the C_{sp^2}–H stretching frequencies were in the range of 20–45 cm^{-1} calculated at the MP2/aug-cc-pVTZ level.[51] Fig. 6 shows that the C_{sp^2}–H blue-shifting of the C_{sp^2}–H···O hydrogen bonds is observed in all dimers, regardless of the electron effect of the substituents, in which the electron-donating derivatives exhibit a stronger C_{sp^2}–H blue-shift compared to electron-withdrawing ones. The smaller magnitude of the C_{sp^2}–H blue-shift in the nonconventional hydrogen bonds was also found in the complexes of XCHO with HF, H_2Z and H_2O (with X = H, F, Cl, Br or CH_3, and Z = O, S, Se or Te). The **2CH_3-O** dimer in this work shows the strongest blue-shift with a $\Delta\nu(C_{sp^2}\text{–H})$ value of *ca.* 53 cm^{-1} (*cf.* Table S9†). Large C_{sp^2}–H blue-shifts of $CH_3CHO\cdots H_2O$ (52 cm^{-1}) and $CH_3CHO\cdots HCOOH$ (96 cm^{-1}) have been reported.[46,62] A very large C_{sp^2}–H blue-shift of the stretching frequency up to 104.5 cm^{-1} was also found in $CH_3CHO\cdots FCOOH$ calculated at the MP2/6-311++G(3df,2pd) level.[54] Consequently, the substitution of one CH_3CHO molecule in the dimer of CH_3CHO by one carboxylic acid, like HCOOH or FCOOH, induces a significant increase in the magnitude of the C_{sp^2}–H stretching frequency blue-shift upon complexation. As seen in Table 1, the polarity of C_{sp^2}–H in the F/Cl/BrCHO monomers is greater than that in the H/CH_3/NH_2CHO ones. This suggests that following complexation, the less polar C_{sp^2}–H bond in the isolated monomer causes a larger magnitude of the C_{sp^2}–H blue-shift and *vice versa*.

4. Concluding remarks

The stable structures of **2R-Z** dimers (R = H, F, Cl, Br, CH_3 or NH_2 and Z = O, S, Se or Te) were found on the potential energy surface. It is notable that the stability of the dimers increases when replacing H in **2H-Z** with both electron-withdrawing and electron-donating groups, and decreases upon changing Z from O to S, Se and Te. This implies an important role of the O atom compared to the S, Se and Te ones in the strength of the nonconventional C_{sp^2}–H···Z hydrogen bonds and dimers. The greater electrostatic attraction of O···H than S/Se/Te···H leads to the stronger strength of **2R-O** compared to **2R-S/Se/Te** in most cases. In contrast, a dominant role of intermolecular electron transfer is the reason for the stronger stability of **2NH_2-S/Se/Te** relative to **2NH_2-O**. Remarkably, while the electrostatic component contributes significantly to the strength of **2R-O/S/Se**, a dominant role of the induction term is observed in **2R-Te**, which has been rarely observed.

The strength of the nonconventional hydrogen bonds lessens in the order of C_{sp^2}–H···O > C_{sp^2}–H···S > C_{sp^2}–H···Se > C_{sp^2}–H···Te, which indeed ranges from −8.1 to −11.0 kJ mol^{-1} for C_{sp^2}–H···O and from −4.7 to −9.3 kJ mol^{-1} for C_{sp^2}–H···S/Se/Te. Hydrogen bonds are mainly stabilized by both the electrostatic interaction between the H and Z atoms and the intermolecular electron density transfer from n(Z) to the σ*(C1–H2) orbital. Besides, replacing H in **2H-S/Se/Te** by electron-donating and -withdrawing groups results in an improvement in the nonconventional hydrogen bond strength, except for the F substituent, which causes an opposite effect.

It is found that a C_{sp^2}–H stretching frequency red-shift is observed in nonconventional C_{sp^2}–H···S/Se/Te hydrogen bonds, while the C_{sp^2}–H···O ones display a blue-shifting of their stretching frequency following complexation. When Z changes from O *via* S to Se and then to Te, the C_{sp^2}–H blue-shift in the nonconventional C_{sp^2}–H···Z hydrogen bonds tends to decrease gradually and eventually turn to a red-shift, in agreement with the enhancement of the proton affinity at the Z site in the order

of O < S < Se < Te. In addition, a rearrangement of electron density in the dimers induces an enhancement of the C_{sp^2}–H red-shift in the sequence of substituents F < CH_3 < H < Cl < Br < NH_2. The magnitude of C_{sp^2}–H stretching frequency red-shift in C_{sp^2}–H···S/Se/Te increases in line with the enhancement of the proton affinity at the Z site and the polarity of the C_{sp^2}–H covalent bond in the isolated monomer. Noticeably, the C_{sp^2}–H blue-shifting of nonconventional C_{sp^2}–H···O hydrogen bonds is weaker for electron-withdrawing substituents than electron-donating ones.

Conflicts of interest

There are no conflicts to declare.

Acknowledgements

This research was funded by Vietnam Ministry of Education and Training (MOET) under grant number B2024-DQN-01.

References

1 I. G. Kaplan, *Intermolecular Interactions: Physical Picture, Computational Methods and Model Potentials*, John Wiley & Sons, 2006.
2 G. R. Desiraju and T. Steiner, *The Weak Hydrogen Bond: in Structural Chemistry and Biology*, Oxford University Press, 2001.
3 C. Tapeinos and A. Pandit, *Adv. Mater.*, 2016, **28**, 5553–5585.
4 R. E. Plata, D. E. Hill, B. E. Haines, D. G. Musaev, L. Chu, D. P. Hickey and D. G. Blackmond, *J. Am. Chem. Soc.*, 2017, **139**, 9238–9245.
5 R. Ghosh, J. A. Mondal and D. K. Palit, *J. Phys. Chem. B*, 2010, **114**, 12129–12143.
6 A. C. C. Carlsson, M. R. Scholfield, R. K. Rowe, M. C. Ford, A. T. Alexander, R. A. Mehl and P. S. Ho, *Biochemistry*, 2018, **57**, 4135–4147.
7 S. J. Grabowski, *Hydrogen Bonding – New Insights*, ed. S. J. Grabowski, Springer, Dordrecht, 2006.
8 Y. Mandel-Gutfreund, H. Margalit, R. L. Jernigan and V. B. Zhurkin, *J. Mol. Biol.*, 1998, **277**, 1129–1140.
9 J. J. Dom, B. Michielsen, B. U. Maes, W. A. Herrebout and B. J. Van der Veken, *Chem. Phys. Lett.*, 2009, **469**, 85–89.
10 J. M. Hermida-Ramón and A. M. Graña, *J. Comput. Chem.*, 2007, **28**, 540–546.
11 S. Hoshika, I. Singh, C. Switzer, R. W. Molt Jr, N. A. Leal, M. J. Kim and S. A. Benner, *J. Am. Chem. Soc.*, 2018, **140**, 11655–11660.
12 J. Yang, Y. Zhang, H. C. F. Wong, J. Huang, Y. L. S. Tse and Y. Y. Yeung, *ACS Catal.*, 2024, **14**, 3018–3027.
13 L. S. Sremaniak, J. L. Whitten, M. J. Truitt and J. L. White, *J. Phys. Chem. B*, 2006, **110**, 20762–20764.
14 R. E. Plata, D. E. Hill, B. E. Haines, D. G. Musaev, L. Chu, D. P. Hickey and D. G. Blackmond, *J. Am. Chem. Soc.*, 2017, **139**, 9238–9245.
15 M. Wohlert, T. Benselfelt, L. Wågberg, I. Furó, L. A. Berglund and J. Wohlert, *Cellulose*, 2022, **29**, 1–23.
16 L. Sobczyk, S. J. Grabowski and T. M. Krygowski, *Chem. Rev.*, 2005, **105**, 3513–3560.
17 S. Scheiner, *J. Indian Inst. Sci.*, 2020, **100**, 61–76.
18 J. Perlstein, *The Weak Hydrogen Bond in Structural Chemistry and Biology*, Oxford University Press, Oxford, New York, 1999.
19 J. Dutta, D. K. Sahoo, S. Jena, K. D. Tulsiyan and H. S. Biswal, *Phys. Chem. Chem. Phys.*, 2020, **22**, 8988–8997.
20 L. Pauling, *J. Am. Chem. Soc.*, 1931, **53**, 1367–1400.
21 G. Trudeau, J. M. Dumas, P. Dupuis, M. Guérin and C. Sandorfy, in *Van der Waals systems*, Springer, Berlin, Heidelberg, 1980, vol. 93, pp. 91–125.
22 I. V. Alabugin, M. Manoharan, S. Peabody and F. Weinhold, *J. Am. Chem. Soc.*, 2003, **125**, 5973–5987.
23 S. N. Delanoye, W. A. Herrebout and B. J. Van der Veken, *J. Am. Chem. Soc.*, 2002, **124**, 7490–7498.
24 W. Wang, Y. Zhang and B. Ji, *J. Phys. Chem. A*, 2010, **114**, 7257–7260.
25 X. Chang, Y. Zhang, X. Weng, P. Su, W. Wu and Y. Mo, *J. Phys. Chem. A*, 2016, **120**, 2749–2756.
26 T. S. Thakur, M. T. Kirchner, D. Bläser, R. Boese and G. R. Desiraju, *Phys. Chem. Chem. Phys.*, 2011, **13**, 14076–14091.
27 A. Kovács, A. Szabó, D. Nemcsok and I. Hargittai, *J. Phys. Chem. A*, 2002, **106**, 5671–5678.
28 I. V. Alabugin, M. Manoharan, S. Peabody and F. Weinhold, *J. Am. Chem. Soc.*, 2003, **125**, 5973–5987.
29 L. Pejov and K. Hermansson, *J. Chem. Phys.*, 2003, **119**, 313–324.
30 Y. Gu, T. Kar and S. Scheiner, *J. Am. Chem. Soc.*, 1999, **121**, 9411–9422.
31 Y. Mao and M. Head-Gordon, *J. Phys. Chem. Lett.*, 2019, **10**, 3899–3905.
32 C. Wang, D. Danovich, S. Shaik and Y. Mo, *J. Chem. Theory Comput.*, 2017, **13**, 1626–1637.
33 S. Shaik, D. Danovich and R. N. Zare, *J. Am. Chem. Soc.*, 2023, **145**, 20132–20140.
34 N. T. Trung, T. T. Hue and M. T. Nguyen, *Phys. Chem. Chem. Phys.*, 2009, **11**, 926–933.
35 N. T. Trung, T. T. Hue, M. T. Nguyen and T. Zeegers-Huyskens, *Phys. Chem. Chem. Phys.*, 2008, **10**, 5105–5113.
36 S. Michielssens, N. T. Trung, M. Froeyen, P. Herdewijn, M. T. Nguyen and A. Ceulemans, *Phys. Chem. Chem. Phys.*, 2009, **11**, 7274–7285.
37 N. T. Trung, T. T. Hue and M. T. Nguyen, *Can. J. Chem.*, 2010, **88**, 849–857.
38 N. T. Trung, T. T. Hue and M. T. Nguyen, *J. Phys. Chem. A*, 2009, **113**, 3245–3253.
39 H. Liu, R. Man, Z. Wang, J. Liao, X. Li, S. Ma, P. Yi and J. Comput, *Biophys. Chem.*, 2014, **13**, 1450037.
40 I. Alkorta and A. Legon, *J. Phys. Chem. A*, 2023, **127**, 4715–4723.
41 B. Reimann, K. Buchhold, S. Vaupel, B. Brutschy, Z. Havlas, V. Špirko and P. Hobza, *J. Phys. Chem. A*, 2001, **105**, 5560–5566.
42 B. Reimann, K. Buchhold, S. Vaupel and B. Brutschy, *Z. Phys. Chem.*, 2001, **215**, 777–793.

43 B. G. Oliveira, R. C. M. U. de Araujo and M. N. Ramos, *J. Mol. Struct.*, 2009, **908**, 79–83.
44 P. Hobza and Z. Havlas, *Chem. Phys. Lett.*, 1999, **303**, 447–452.
45 R. Gopi, N. Ramanathan and K. Sundararajan, *Chem. Phys.*, 2016, **476**, 36–45.
46 N. T. Trung, P. N. Khanh, A. J. P. Carvalho and M. T. Nguyen, *J. Comput. Chem.*, 2019, **40**, 1387–1400.
47 A. K. Chandra and T. Zeegers-Huyskens, *J. Comput. Chem.*, 2012, **33**, 1131–1141.
48 A. Bhattacherjee and S. Wategaonkar, *Phys. Chem. Chem. Phys.*, 2016, **18**, 27745–27749.
49 E. Van Dornshuld, C. M. Holy and G. S. Tschumper, *J. Phys. Chem. A*, 2014, **118**, 3376–3385.
50 W. Li, C. Pérez, A. L. Steber, M. Schnell, D. Lv, G. Wang, X. Jeng and M. Zhou, *J. Am. Chem. Soc.*, 2023, **145**, 4119–4128.
51 A. Karpfen and E. S. Kryachko, *J. Phys. Chem. A*, 2007, **111**, 8177–8187.
52 A. Chand, D. K. Sahoo, A. Rana, S. Jena and H. S. Biswal, *Acc. Chem. Res.*, 2020, **53**, 1580–1592.
53 A. Chand and H. S. Biswal, *J. Indian Inst. Sci.*, 2020, **100**, 77–100.
54 N. T. An, N. T. Duong, N. N. Tri and N. T. Trung, *RSC Adv.*, 2022, **12**, 35309–35319.
55 A. Rana, D. Pal and S. Chakraboty, *Indian J. Phys.*, 2024, 1–9.
56 P. Chopra and S. Chakraborty, *Chem. Phys.*, 2018, **500**, 54–61.
57 D. Pal, H. Charaya and S. Chakraborty, *ChemPhysChem*, 2023, e202300124.
58 K. K. Mishra, S. K. Singh, S. Kumar, G. Singh, B. Sarkar, M. S. Madhusudhan and A. Das, *J. Phys. Chem. A*, 2019, **123**, 5995–6002.
59 K. K. Mishra, S. K. Singh, P. Ghosh, D. Ghosh and A. Das, *Phys. Chem. Chem. Phys.*, 2017, **19**, 24179–24187.
60 V. R. Mundlapati, D. K. Sahoo, S. Ghosh, U. K. Purame, S. Pandey, R. Acharya and H. S. Biswal, *J. Phys. Chem. Lett.*, 2017, **8**, 794–800.
61 N. T. T. Cuc, N. T. An, V. T. Ngan, A. K. Chandra and N. T. Trung, *RSC Adv.*, 2022, **12**, 1998–2008.
62 N. T. T. Cuc, C. T. D. Phan, N. T. A. Nhung, M. T. Nguyen, N. T. Trung and V. T. Ngan, *J. Phys. Chem. A*, 2021, **125**, 10291–10302.
63 M. J. Frisch, G. W. Trucks, H. B. Schlegel, *et al.*, *Gaussian 16 Rev. A. 03*, Gaussian Inc., Wallingford CT, 2016.
64 R. F. Bader, *Chem. Rev.*, 1991, **91**, 893–928.
65 M. Ziółkowski, S. J. Grabowski and J. Leszczynski, *J. Phys. Chem. A*, 2006, **110**, 6514–6521.
66 R. F. Bader, *Acc. Chem. Res.*, 1985, **18**, 9–15.
67 E. Espinosa, E. Molins and C. Lecomte, *Chem. Phys. Lett.*, 1998, **285**, 170.
68 E. D. Glendening, C. R. Landis and F. Weinhold, *J. Comput. Chem.*, 2019, **40**, 2234–2241.
69 A. Amonov and S. Scheiner, *Phys. Chem. Chem. Phys.*, 2023, **25**, 23530–23537.
70 J. Contreras-García, E. R. Johnson, S. Keinan, R. Chaudret, J. P. Piquemal, D. N. Beratan and W. Yang, *J. Chem. Theory Comput.*, 2011, **7**, 625–632.
71 *Chemical Applications of Atomic and Molecular Electrostatic Potentials: Reactivity, Structure, Scattering, and Energetics of Organic, Inorganic, and Biological Systems*, ed. P. Politzer and D. G. Truhlar, Springer Science & Business Media, 2013.
72 B. Jeziorski, R. Moszynski and K. Szalewicz, *Chem. Rev.*, 1994, **94**, 1887–1930.
73 J. M. Turney, A. C. Simmonett, R. M. Parrish, E. G. Hohenstein, F. A. Evangelista, J. T. Fermann, B. J. Mintz, L. A. Burns, J. J. Wilke, M. L. Abrams, N. J. Russ, M. L. Leininger, C. L. Janssen, E. T. Seidl, W. D. Allen, H. F. Schaefer, R. A. King, E. F. Valeev, C. D. Sherrill and T. D. Crawford, *Wiley Interdiscip. Rev.: Comput. Mol. Sci.*, 2012, **2**, 556–565.
74 U. Koch and P. L. Popelier, *J. Phys. Chem.*, 1995, **99**, 9747–9754.
75 K. K. Murray, T. M. Miller, D. G. Leopold and W. C. Lineberger, *J. Chem. Phys.*, 1986, **84**, 2520–2525.
76 K. Kimura, *Handbook of HeI Photoelectron Spectra of Fundamental Organic Molecules*, Halsted Press, 1981.
77 M. R. Nimlos, J. A. Soderquist and G. B. Ellison, *J. Am. Chem. Soc.*, 1989, **111**, 7675–7681.
78 E. P. Hunter and S. G. Lias, *J. Phys. Chem. Ref. Data*, 1998, **27**, 413–656.